Formation and Environmental Context of Giant Bulgeless Disk Galaxies in the Early Universe: Insights from Cosmological Simulations

1 Supplementary Information

Here, we further compare the properties of giant bulgeless disks (GBDs) and those of normal disk galaxies in the same mass range (non-GBDs). First, we examine the radial profiles, including age specific star formation rate, gas-phase metallicity[1], and the two-component Toomre Q parameter. Second, to identify the most important halo and environmental factors that drive GBD formation, we analyze the distributions of these quantities in the spaces spanned by morphological parameters. In particular, we consider size, disk mass fraction $f_{\rm disk}$, and bulge mass fraction $f_{\rm bulge}$.

1.1 Radial profiles

In Supplementary Fig. 1, we present the radial profiles of GBDs and non-GBDs at $z = 1, 2, 3$. Overall, the GBDs exhibit younger stellar populations, higher sSFR, and lower gas-phase metallicities. Closer examination reveals that the GBDs also show distinct shapes in the profiles – they have two components separated at $r \sim 0.6 - 0.9\, r_{1/2}$. Notably, their age profiles exhibit a young stellar population in the outer region at $\sim 2r_{1/2}$. There is an older stellar population around $0.3 - 0.6r_{1/2}$, whereas the innermost part within $\sim 0.3r_{1/2}$ is relatively young again. This "N-shaped" behavior (from inner part to the outskirt) is particularly obvious at $z = 2$, and qualitatively holds at other epochs as well. The sSFR profiles of GBDs show consistent behaviors, with double peaks in both inner and outer parts, at $\sim 0.3r_{1/2}$ and $\sim 2r_{1/2}$, respectively. In contrast, non-GBDs exhibit positive radial sSFR gradients, with suppressed star formation in their centers. The inner sSFR peak corresponds nicely to the inner disks, which we find to be a universal feature in high-z GBDs, as illustrated in the paper. The gas-phase metallicity profile of non-GBDs follows a broken power law with a characteristic scale at $r \sim 0.4r_{1/2}$, whereas GBDs seem to show two bumps in the profile, at $r \sim 0.2r_{1/2}$ and $\sim 2r_{1/2}$, respectively. All these features collectively reveal that GBDs host relatively young inner disks, besides an extended outer disk – a unique feature that is worth theoretical and observational follow-ups.

[1]The gas-phase metallicity is defined as log(O/H)+12, measured as the number ratio between oxygen and hydrogen atoms in logarithmic scale. The mass fraction of oxygen and hydrogen in each gas cell are obtained using `GFM_Metals`. The number fraction is then converted by the nucleus number of H and O, 1 and 16.

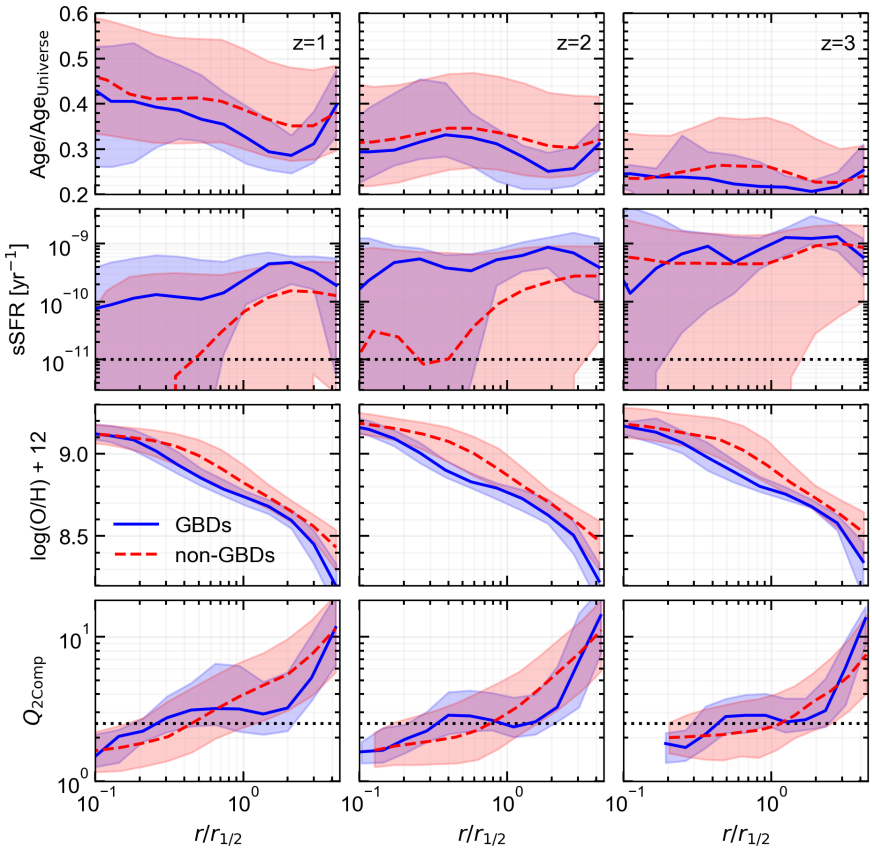

Supplementary Fig. 1: **Radial profiles for GBDs and normal disk galaxies of similar mass (non-GBDs) at redshifts up to 3.** *First row:* Stellar age normalized by the universe age at each redshift. *Second row:* Specific star formation rate, sSFR, obtained by star formation rate of gas particles at each bin and stellar mass in the same bin. The horizontal black dotted lines represent the quenching threshold of sSFR=10^{-11}yr^{-1}. *Third row:* Gas phase metallicity, log(O/H)+12. *Fourth row:* Two-component Toomre stability index, $Q_{2\mathrm{Comp}}$. The horizontal black dotted lines indicate $Q_{\mathrm{crit}} = 2.5$, an approximate stability threshold according to various simulation studies (see references in the paper). The median profiles of GBDs and non-GBDs are represented by blue and red lines, respectively, with the shaded areas indicating 16th and 84th percentiles. **The GBDs are generally younger, with higher star-formation rate, and lower metallicity compared to non-GBDs, and are marginally stable. They seem to show two relatively young components at $\sim 0.3r_{1/2}$ and $\sim 2r_{1/2}$.**

As we discussed in the paper, the $Q_{2\mathrm{Comp}}$ profiles of GBDs are quite flat at $\sim 2-3$ within $\sim 2r_{1/2}$. This manifests a marginally stable status that can lead to clump

formation later on, consistent with the fact that $f_{\rm disk}$ decreases towards lower redshifts before any major merger occurs. GBDs are less stable in the outer disks at $r \sim 2r_{1/2}$ compared to non-GBDs, the latter of which show monotonically increasing $Q_{\rm 2Comp}$ with radius.

1.2 Feature importance

To identify the key factors for GBD formation, we examine the distributions of relevant factors in the $\Delta \log r_{1/2}$ - $f_{\rm disk}$ plane and the $\Delta \log r_{1/2}$ - $f_{\rm bulge}$ plane, shown in Supplementary Figs. 2 to 7. We mainly focus on $\Delta \log r_{1/2}$ - $f_{\rm disk}$, since $\Delta \log r_{1/2}$ - $f_{\rm bulge}$ yields basically the same qualitative conclusion. Here, galaxy size $\Delta \log r_{1/2}$ is defined as the offset of the logarithmic half-stellar-mass radius with respect to the median value (for galaxies with the same stellar mass at the same redshift). To assess the correlation between morphology and factor X, we compute the three-dimensional correlation coefficient, defined as

$$\mathcal{R}^2 = \frac{\mathcal{R}^2_{X,r_{1/2}} + \mathcal{R}^2_{X,f} - 2\mathcal{R}_{X,r_{1/2}}\mathcal{R}_{X,f}\mathcal{R}_{r_{1/2},f}}{1 - \mathcal{R}^2_{r_{1/2},f}} \tag{1}$$

where f can be disk fraction $f_{\rm disk}$ or bulge fraction $f_{\rm bulge}$, and $\mathcal{R}_{i,j}$ is the Pearson correlation coefficient between quantity i and quantity j. To better evaluate whether X is correlated or anti-correlated with both size and mass fraction, or correlated with one and anti-correlated with the other, we multiply the correlation coefficient $\mathcal{R}$ by $\mathrm{Sign}(\mathcal{R}_{X,r_{1/2}}\mathcal{R}_{X,f})$. Positive values indicate that X is correlated with both size and mass fraction, while negative values mean that X is correlated with one and anti-correlated with the other.

From Supplementary Fig. 2 to Supplementary Fig. 4, we examine the $\Delta \log r_{1/2}$ - $f_{\rm disk}$ plane. We highlight the region with $f_{\rm disk} \geq 0.8$ and $\Delta \log r_{1/2} \geq 0.25$, which approximately corresponds to GBDs. If a quantity X is key to GBD formation, its highest (or lowest) values are expected to correspond to large $\Delta \log r_{1/2}$ and high $f_{\rm disk}$, rendering a diagonal trend.

In the first row, we examine the *dark-halo properties*. The halo concentration parameter c shows anti-diagonal trend, with lower values held by galaxies with larger size but smaller disk fraction. The trend of the Einasto-profile index α evolves with redshift: at $z = 3$, it follows an anti-diagonal pattern, while at $z = 2$ and 1, the trend shifts to vertical and diagonal, respectively, with higher values found in larger galaxies. While the α trends are strong, we caution that it may be more of a baryonic effect, in the sense that more compact galaxies cause stronger halo contraction thus lower α. We thus caution against interpreting high α as a cause for GBD formation. The axis-ratio q shows somewhat random distributions. However, at $z = 2$ and 3, the GBD regime has large q values. Finally, the spin parameter λ shows basically vertical trends, with larger values for galaxies of larger sizes.

In the second row, we examine the *environmental factors* in terms of the alignment of CGM, the alignment of mergers, and large-scale number density. The three alignment angles exhibit clear diagonal trends across redshifts, with higher cosine values (better alignment) found in galaxies with larger sizes and higher disk fractions. In the

last panel of the second row, we show the trend of the number density of neighbours within 3 Mpc, $n_{3\mathrm{Mpc}}$. While the correlation is somewhat weak and the direction of the overall trend is not as clear, the GBD regime has some of the lowest number densities. As discussed in the paper, high-z massive systems all populate high-density peaks, so the lower $n_{3\mathrm{Mpc}}$ for GBDs simply indicates that they reside in proto-clusters or cosmic knots forming in action.

In the last row, we examine *merger statistics*. Galaxies that experienced mergers that are more cold-gas rich tend to have higher disk fractions. Similarly, galaxies with quiescent merger histories also have higher disk fractions. However, no clear diagonal trend is observed.

Overall, coherent CGM and mergers show the most clear diagonal trend in the $\Delta \log r_{1/2}$ - f_{disk} space and are thus likely the most important factors for GBD formation. Dark-matter halo structures, especially lower concentration c and higher spin λ, also play an important role in driving disks large, but do not necessarily prevent bulge formation. High cold-gas fraction in mergers and quiescent merger histories contribute to high disk fractions.

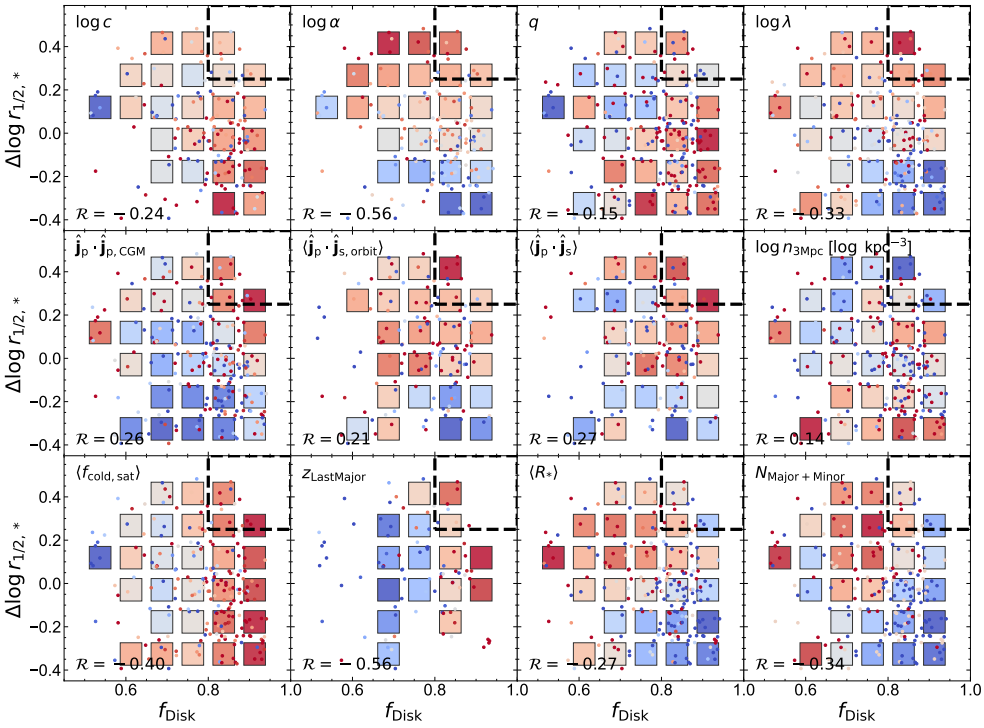

Supplementary Fig. 2: **Diagnostics of the importance of relevant actors for GBD formation**, in terms of their distributions in the $\Delta \log r_{1/2}$ - $f_{\rm disk}$ plane, at $z = 3$ in the TNG100 simulation, including *dark-matter-halo properties* (concentration c, Einasto-profile shapeα, axis ratio q, spin λ), the *metrics for alignment* between the galaxy and hosting CGM or merging satellites (instantaneous cosine of the angle between the galaxy's angular-momentum vector and the angular-momentum of the hosting CGM $\hat{\boldsymbol{j}}_{\rm p} \cdot \hat{\boldsymbol{j}}_{\rm p,CGM}$, the average cosine of the angle between the angular-momentum vector of the galaxy and the orbital angular-momentum of a merging satellite $\langle \hat{\boldsymbol{j}}_{\rm p} \cdot \hat{\boldsymbol{j}}_{\rm s,orbit} \rangle$, and the average cosine of the angle between the angular-momentum vector of the galaxy and that of a merging satellite $\langle \hat{\boldsymbol{j}}_{\rm p} \cdot \hat{\boldsymbol{j}}_{\rm s} \rangle$, where average cosine values are stellar-mass weighted, for all the mergers during the last 4 dynamical times that penetrated within $10 r_{1/2}$), the *large-scale number density* (number density within 3 Mpc, $n_{\rm 3Mpc}$, of all the neighbouring halos with masses exceeding 0.1% of the halo of interest), and *merger statistics* (average cold gas fraction of all the mergers in the past, $\langle f_{\rm cold,sat} \rangle$, redshift of last major merger $z_{\rm LastMajor}$, average stellar mass ratio of all the mergers $\langle R_* \rangle$, and the number of major and minor mergers $N_{\rm Major+Minor}$ during the last 4 dynamical times). The color of a square represents the mean value of galaxies within a box of 0.11 dex in $f_{\rm disk}$ and 0.22 dex in $\Delta \log r_{1/2}$ around the center position of each square, calculated from at least 10 samples – bluer means lower values and redder means stronger values. These mean values are obtained using locally weighted regression smoothing in Python package `LOESS`. The colors of the individual data points show the unsmoothed values, using the same color scale as the squares. The multiple correlation coefficients are displayed in the lower-left corners. The black dashed rectangle highlights the regime that corresponds roughly to GBDs.

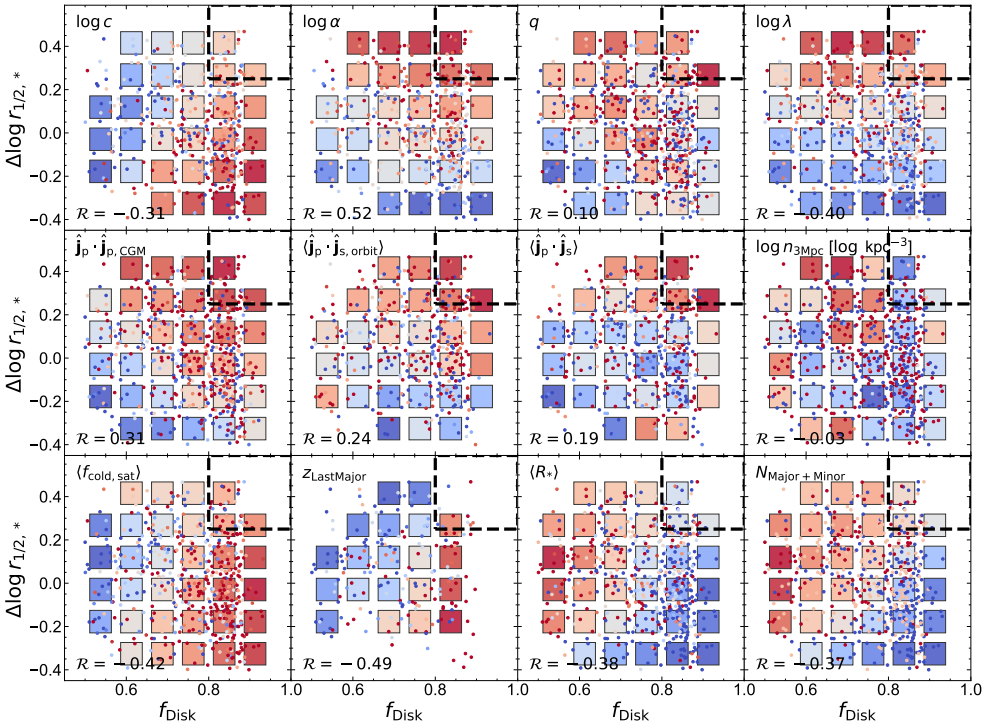

Supplementary Fig. 3: Same as Supplementary Fig. 2, but for $z = 2$, and the average is taken over 10 galaxies (instead of 5) for each square.

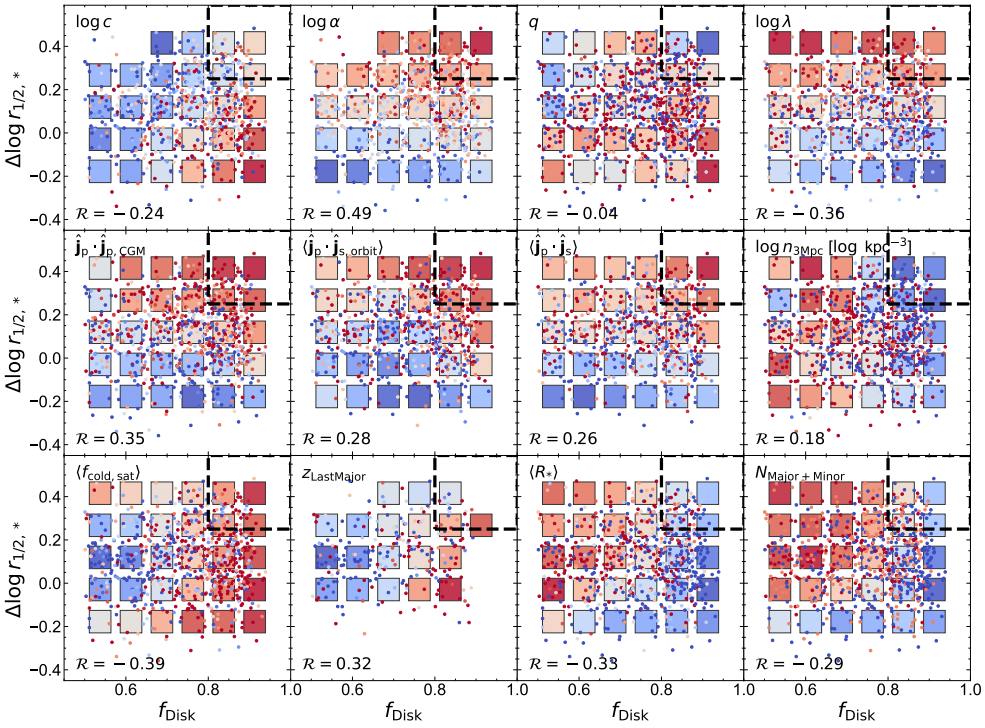

Supplementary Fig. 4: Same as Supplementary Fig. 3 but for $z = 1$.

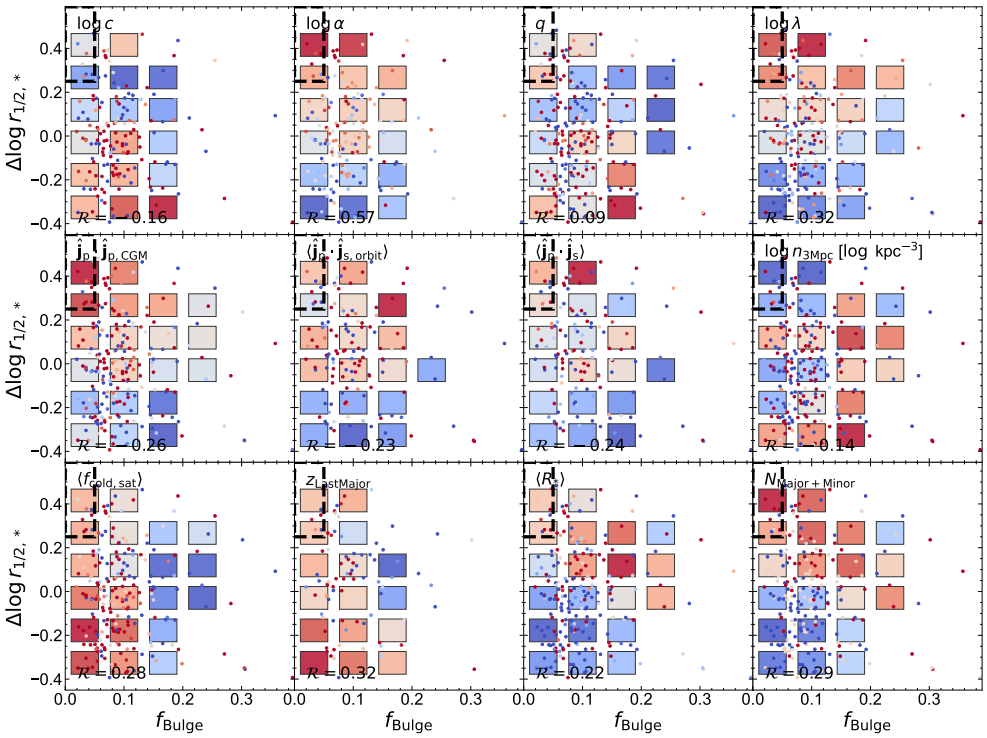

Supplementary Fig. 5: Similar to Supplementary Fig. 2, but for the $\Delta \log r_{1/2}$ - $f_{\rm bulge}$ space.

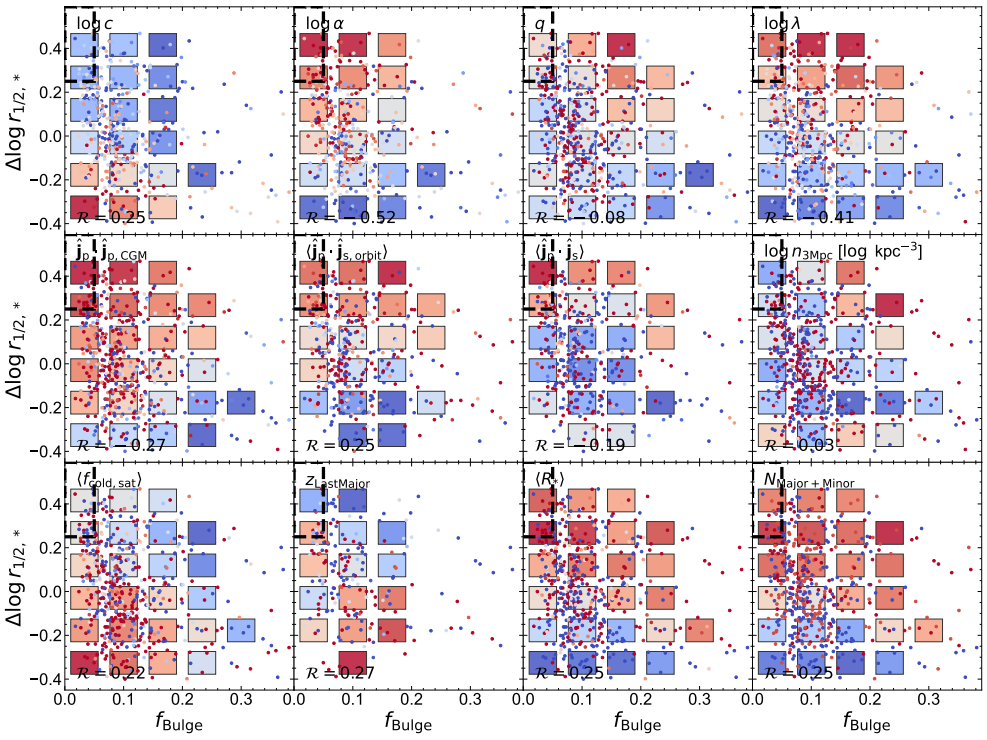

Supplementary Fig. 6: Similar to Supplementary Fig. 3, but for the $\Delta \log r_{1/2}$ - $f_{\rm bulge}$ space.

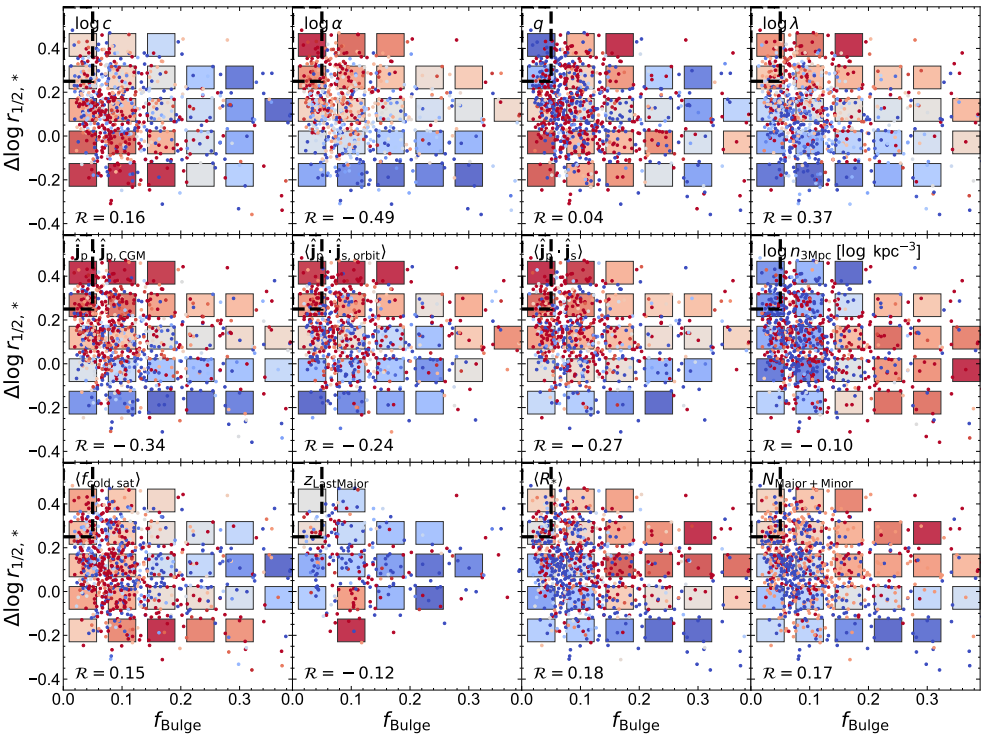

Supplementary Fig. 7: Similar to Supplementary Fig. 4, but for the $\Delta \log r_{1/2}$ - $f_{\rm bulge}$ space.